INSTITUTE FOR NUCLEAR STUDY
UNIVERSITY OF TOKYO
Tanashi, Tokyo 188
Japan



INS-Rep.-577
March 1986

# Nucleus-Nucleus Scattering and Interaction Radii of Stable and Unstatble Nuclei

H. Sato

and

Y. Okuhara

INS-Rep.-577
March 1986

# Nucleus-Nucleus Scattering and Interaction Radii of Stable and Unstatble Nuclei

H. Sato
Institute for Nuclear Study, University of Tokyo,
Tanashi, Tokyo 188, JAPAN
and
Y. Okuhara
Department of Physics, Queen's University,
Kingston, Ontario, CANADA.

**Abstract:**

The interaction cross sections of medium and high energy nucleus-nucleus scattering are studied with the Glauber Model and Hartree-Fock type variational calculation. The interaction cross sections so obtained nicely satisfy the additivity relationship, which in turn suggests the existence of a nuclear interaction radius in nucleus-nucleus scattering. With the calculated interaction cross sections, the nuclear interaction mean free path of high energy nucleus in emulsion is studied, and the results agree very well with experimental data. It is found that the interaction radius of the projectile nucleus can also be determined from emulsion experiment.

## I. Introduction

The determination of nuclear size is one of the most important problems in nuclear physics. Thus far various experimental methods ( Coulomb displacement energy, high energy electron scattering, X-rays from muonic atoms and pion, proton and alpha scatterings ) have been employed to determine the nuclear size. The radii of proton and neutron together with their distributions have been determined with these experiments and compared with available theoretical nuclear structure calculations. However, due to experimental restriction on the choice of the target, these measurements have thus far been limited to the case of stable nuclei. Recently, Tanihata et al ( INS-LBL Collaborations ) have succeeded in determining the interaction cross sections for scattering of light stable and unstable nuclei from stable target nucleus with the use of the secondary isotope beams produced by the Bevalac heavy ion beam[1,2]. In a previous paper[3], we have studied the interaction cross sections by performing a Glauber model calculation using density dependent Hartree Fock ( DDHF ) type variational calculation of the nuclear density distribution, and we found nice agreement between the theoretical and experimental interaction cross sections. However, it is not entirely clear which part of the nuclear radial distribution is responsible for the interaction cross sections measured. Therefore, in this paper, it is our aim to study the relationship between the interaction cross sections and nuclear matter distribu-

tion, and, examine the additivity relationship of the interaction cross sections[1]. We find that the additivity relationship is numerically well satisfied for almost all the combinations of nuclei considered. The validity of the additivity relationship suggests the existence of an interaction radius which can be considered to be an energy independent characteristic nuclear radius in nucleus-nucleus scattering ( analogous to the charge radius as determined from electron scattering ). As an application of our analysis we study the nuclear interaction mean free path in emulsion, and show that the interaction radius can also be determined with the emulsion experiment.

In section II we show the method of calculation of the cross sections. Then we present the numerical results and study the additivity relationship between the interaction cross sections in section III. In section IV we study the nuclear interaction mean free path as an application. We discuss and summarize the work in section V.

## II. Calculation of the cross sections

### II-1. Calculation of nuclear matter distribution

To derive the nuclear density distribution of both closed shell and middle of shell nuclei, we employ the Hartree-Fock type variational method, which has been used by Yazaki in the study of the systematics of the core and single particle properties of sd shell nuclei and Ca isotopes[4]. By minimizing the core plus average shell model

energies as a functional of single particle wave function, the Hartree-Fock like equations for the single particle wave functions of the core ($\mu$) and valence ($\alpha$) nucleon states are obtained as follow[4]

$$( h + U_c + \frac{n}{\Omega} U_v ) \phi_{\alpha(\nu)} = \tilde{\varepsilon}_{\alpha(\nu)} \phi_{\alpha(\nu)} , \qquad (1)$$

where h is the kinetic energy operator. The non-local potentials $U_c$ and $U_v$ for the core and valence nucleons respectively are given by the two-body interactin

$$U_{c(v)}(x,x') = \int dx_1 dx_2 \{ v(x,x_1:x',x_2) - v(x,x_1:x_2,x') \} \times \rho_{c(v)}(x_1,x_2), \qquad (2)$$

with the density matrices $\rho_c$ and $\rho_v$ defined by

$$\rho_c(x,x') = \sum_{\nu} \phi_{\nu}(x) \phi^*_{\nu}(x') \quad \text{and} \quad \rho_v(x,x') = \sum_{\alpha} \phi_{\alpha}(x) \phi^*_{\alpha}(x'). \qquad (3)$$

Here $\Omega$ denotes the number of valence single particle states and n is the number of valence nucleons. For the two-body effective interaction we employ the Skyrme ( SK ) interactions[5]. The root mean square ( rms ) proton, neutron and matter radii for nuclei are calculated using the single particle wave functions obtained in such a way that $r_{rms} = \sqrt{\langle r^2 \rangle - \frac{3}{2} b^2/A}$ [6,7]. We find that the single particle energies and the rms radii obtained are quite similar to those obtained by just plugging in the proton and mass num-

bers in the DDHF program[8]. Since it is an interesting question to ask whether the bound $^{10}$He exists, we study the systematics of He-isotopes by performing the calculations with various Skyrme interactions. It was found that the interactions which have rather weak three-body term ( for instance SKIV, SKV interactions[5] and also DME[7] ) predict bound $^{10}$He nucleus and produce a smaller neutron ( or matter ) radius for $^{8}$He than for $^{6}$He.

II-2. Calculation of total and interaction cross sections

To calculate the cross sections for the nucleus-nucleus scatterings, we perform a Glauber model[9] calculation, taking into account the Pauli principle, center of mass (CM) corrections and effects of higher order collisions[10,11]. The scattering amplitude for collision between nucleus $A_1$ and nucleus $A_2$ can be written as[11]

$$F(q) = \frac{ik}{2\pi}\int d^2b\, e^{i\vec{q}\vec{b}}\left( 1 - e^{i\bar{\chi}_{opt}(\vec{b})} \right), \qquad (4)$$

where $\bar{\chi}_{opt}(\vec{b})$ is the CM corrected optical phase-shift function and it is related to the CM uncorrected phase-shift function $\chi_{opt}(\vec{b})$ by

$$e^{i\bar{\chi}_{opt}(\vec{b})} = (2\pi)^{-2}\int d^2q d^2b' e^{-i\vec{q}(\vec{b}-\vec{b}')} e^{i\chi_{opt}(\vec{b}')} K(q). \qquad (5)$$

Here, the CM correction K(q) is given by the function

$$K(q) = \exp\left\{ q^2 (R_1^2/4A_1 + R_2^2/4A_2) \right\}, \qquad (6)$$

where the parameter $R_i$ is related to the calculated rms matter radius $r_{rms}(A_i)$ as follows

$$R_i^2 = \frac{2A_i}{3(A_i-1)} r_{rms}^2(A_i). \tag{7}$$

The optical phase-shift function $\chi_{opt}(\vec{b})$ is given by

$$i\chi_{opt}(\vec{b}) = \ln\langle\Phi_{A_1}\Phi_{A_2}\Big|\prod_{i=1}^{A_1}\prod_{j=1}^{A_2}\{1-\Gamma_{ij}(\vec{b}-\vec{s}_i+\vec{s}_j')\}\Big|\Phi_{A_1}\Phi_{A_2}\rangle, \tag{8}$$

$$= \ln\langle\Phi_{A_1}\Phi_{A_2}\Big|\ 1-\sum_{ij}\Gamma_{ij}+\sum_{ij}\sum_{kl}\Gamma_{ij}\Gamma_{kl}\ \cdots\Big|\Phi_{A_1}\Phi_{A_2}\rangle, \tag{9}$$

where $\Phi_{A_i}$ is the ground state wave function of the nucleus $A_i$, $\vec{s}_i$ and $\vec{s}_j'$ are the projections of nucleon coordinates on the impact parameter plane, and $\Gamma_{ij}$ are the nucleon-nucleon ( NN ) profile functions. Both phase-shift functions $\bar{\chi}_{opt}(\vec{b})$ and $\chi_{opt}(\vec{b})$ are obtainable by expanding eqs.(5,9) in powers of $\Gamma_{ij}$ such that[11],

$$i\bar{\chi}_{opt}(\vec{b}) = i\sum_j\bar{\chi}_j(\vec{b}) \quad \text{and} \quad i\chi_{opt}(\vec{b}) = i\sum_j\chi_j(\vec{b}). \tag{10}$$

In this work, we retain terms up to second order which are evaluated with the Slater determinant of the single particle wave functions generated with the Hatree-Fock like equation (1). The NN profile function $\Gamma(\vec{b})$ is related to the experimentally measured NN scattering amplitude $f(k_N;\vec{q})$ as follows

$$\Gamma(\vec{b}) = (2\pi ik_N)^{-1}\int d^2q\ e^{-i\vec{q}\vec{b}}f(k_N;\vec{q}), \tag{11}$$

which can then be readily evaluated by using the usual high energy parameterization for the NN scattering amplitude

$$f(k_N;\vec{q}) = \frac{k_N\sigma(i+\rho)}{4} e^{-aq^2/2}, \qquad (12)$$

where the parameters are taken from reference 12).

We note that while it is adequate to use the usual method[6,7] for the CM correction in the calculation of the rms radii and the total binding energy, we need much more consistent and accurate treatment of the CM correction in the nuclear structure calculation because the CM correction plays a very important role in the Glauber model calculation.

## III. Numerical results and additivity relationship

The total and interaction cross sections for the proton-nucleus and nucleus-nucleus scatterings at the incident energy of 0.79 GeV/N are calculated with the SKV interaction. The calculated results corresponding to the first order ($\bar{\chi}_1$) and second order ($\bar{\chi}_2$) collision terms are tabulated in Table 1. The corrections due to the second order collision terms are negative for nucleus-nucleus scatterings, and amount to 6~10 % for the total cross sections and 4~7 % for the interaction cross sections. On the other hand, the corrections are positive for proton-nucleus scatterings amounting to 1~3 % for the total cross sections and 0~2 % for the interaction ones. The correction becomes pro-

gressively smaller as the nucleus involved becomes heavier.

The total and interaction cross sections for proton-nucleus scatterings at 1.00 GeV are calculated with the SKIII and SKV interactions and are compared with experimental data[13] in Table 2. Both SKIII and SKV interactions give almost equivalent total and interaction cross sections, and reproduce the experimental cross sections quite nicely. The interaction cross sections for $^{56}$Fe-nucleus scatterings at 1.88 GeV/N are also calculated and compared with experimental data[14] in Table 3. The experimental interaction cross sections are reproduced within 5 % error for light to heavy target nuclei except S, Ta and U nuclei. The discrepancy, which becomes larger when heavier nuclei are involved, may be caused by the neglect of higher order collision terms. The interaction cross sections for nucleus-nucleus scatterings at 0.79 GeV/N are also calculated with the SKIII and SKV interactions and the results together with experimental values[1,2] are tabulated in Table 4. For the case of $^{12}$C target the results are also summarized in Fig.1. The experimental interaction cross sections are generally well reproduced. In all the cases studied the SKV interaction reproduces the experimental results as observed by Tanihata et al[1,2] better than the SKIII interaction. The overestimation of the cross sections for $^{4}$He-$^{4}$He, $^{4}$He-$^{12}$C and $^{4}$He-$^{27}$Al scatterings can be attributed to the fact that the DDHF calculations usually predict larger rms radii for the $^{4}$He than the experimental value. Therefore, for the

special case of the $^{4}$He nucleus we need a much more accurate nuclear structure calculation. On the other hand, the underestimation of the cross section for $^{11}$Li-$^{12}$C scattering seems harder to understand within the framework of this kind of calculations, nonetheless, nuclear deformation effects may play a role here and this is discussed in section V.

Assuming a simple parameterised formula, $\pi R^2$, for the cross section, we can compare the cross sections with the overlapping of the two radial distributions of the two colliding nuclear matter densities. Then, we find that the total cross sections in general correspond to a position at equivalent to 10% of the central value of nuclear matter distributions except for $^{4}$He nucleus where the cross sections are determined by the position at about twice the central values of the corresponding matter density. The situation is similar for the interaction cross section where it corresponds to a position at about 10% of the central matter density for $^{4}$He nucleus and at about 25~30% for other nuclei. Therefore, these positions and hence cross sections may be considered to be given by a combination of proper invariant nuclear size of each nucleus. This is the reason why the additivity relationship of the cross sections works so well. The additivity relationship of the interaction cross sections[1] is expressed as

$$\sigma_{int}(p,t) = \pi( R_p + R_t )^2, \qquad (13)$$

where $R_p$ and $R_t$ are the interaction radii of the projectile and target nuclei respectively. These interaction radii are defined by the interaction cross sections of identical nuclei in such a way that

$$R_p = \sqrt{\sigma_{int}(p,p)/4\pi} \quad \text{and} \quad R_t = \sqrt{\sigma_{int}(t,t)/4\pi} \,. \qquad (14)$$

The right hand side ( RHS ) and the left hand side ( LHS ) of eq.(13) for interaction cross sections are calculated respectively with the SKV interaction for $^{56}$Fe-nucleus and $^{4}$He-nucleus scatterings at 1.88 GeV/N, and the results are tabulated in Table 5. The discrepancy between the two treatments is much smaller than the corrections due to higher order collision terms. For $^{56}$Fe-nucleus scatterings we find good agreement between the two treatments, especially for medium and heavy target nuclei. However, the discrepancy becomes larger for lighter target nuclei ( $A \leq 12$ ). On the other hand, for $^{4}$He-nucleus scatterings, we find an almost constant ( 3 % ) discrepancy between the two treatments for medium and heavy target nuclei though a decreasing trend may be discerned as target nuclei become smaller. ( In fact the discrepancy becomes zero for $^{4}$He target. ) To examine the extreme case of light nucleus, we also study the proton interaction radius for proton-nucleus scatterings. Here we find that the situation is similar to that of the $^{4}$He-nucleus case though a much larger discrepancy is observed. The proton interaction radius is found to be given by

0.37 fm for p-$^4$He, 0.20 fm for p-1p shell nucleus, 0.15 fm for p-2s1d shell nucleus, 0.10 fm for p-nucleus with A = 50 $\sim$ 150 and 0.05 fm for p-nucleus with A>150 respectively.

Thus we can conclude that the cross sections for nucleus-nucleus scattering are generally well reproduced by the realistic Glauber model calculation using realistic nuclear wave functions. The additivity relationship of inetraction cross sections for nucleus-nucleus scatterings works quite well provided extremely light nuclei are not involved. Therefore it seems not unrealistic to introduce the idea of the interaction radius. The rms matter radii and the interaction radii at 1.88 GeV/n are calculated for various nuclei with the SKV interaction, and the results are tabulated in columns 2, 3, 7 and 8 of Table 6.

## IV. Nuclear interaction mean free path in the emulsion

The nuclear emulsion is one of the most useful and powerful nuclear detectors, and it has played a very important role in finding various elementary particle. However, even though the electro-magnetic behaviour of an energetic charged particle in the emulsion is well known theoretically and experimentally[15], the nuclear interaction mean free path ( IMFP ) of a projectile nucleus in the emulsion is not well known. Thus far no reliable quantitative study on the IMFP exists, and only the empirical formula ($\lambda = A\, z^{-b}$ ) is known[16]. This peculiar fact stems mainly from the diffi-

culty in the calculation of the interaction cross section between the projectile and the target nuclei ( nuclear components of the emulsion ). Since we have now a reliable method to calculate the interaction cross sections of nucleus-nucleus scattering, we shall study the IMFP here.

The IMFP $\lambda_p$ of the projectile nucleus in the emulsion is given by

$$1/\lambda_p = \sum n_i \sigma_{int}(p,i), \tag{15}$$

where $n_i$ is the composition of the nuclear component i in the emulsion and $\sigma_{int}(p,i)$ is the interaction cross section between the projectile nucleus and the target nucleus i. With eq.(13), we can express eq.(15) by

$$1/\lambda_p = AR_p^2 + BR_p + C, \tag{16}$$

with

$$A = \pi \sum_i n_i \ , \ B = 2\pi \sum_i n_i R_i \ , \text{ and } C = \pi \sum_i n_i R_i^2 \ . \tag{17}$$

The coefficients A, B and C at 1.88 GeV/N are calculated for typical emulsions Ilford G5 and Fuji ET7B[17] and are tabulated in Table 7. To examine the energy dependence of A, B and C, we perform the calculation at several incident energies ( 0.79 ~ 2.1 GeV/N ). We find that the energy dependence is very small ( typically 1% less for B and 2% less for

C at 0.87 GeV/N ). The IMFPs calculated for various nuclei are tabulated in columns 4, 5, 9 and 10 of Table 6. Proton IMFP $\lambda_p$ = 32.7cm and $\lambda_p$ = 32.6cm for the Ilford G5 and Fuji ET7B respectively are also obtained. In Fig. 2 we compare the calculated IMFPs in the Ilford G5 for 1.8 GeV/N projectiles with the experimental IMFPs obtained with $^{40}$Ar beam[18]. There is good agreement.

We note here the important implication of the isotope-dependence of the interaction radius of the projectile ($R_p$) as indicated in Table 6[19]. Since the IMFP is given by a simple quadratic function of $R_p$, the isotope-dependence of the IMFP may be correspondingly observed in the emulsion, especially for the light nuclei. Therefore, in view of the isotope-dependence it is quite inadequate to analyze the experimental IMFP in terms of the Z=1 converted phenomena ($\Lambda$) with the formula $\Lambda = \lambda Z^b$, and this formula may sometimes lead to misunderstanding.

The nice agreement between calculated and experimental IMFPs suggests the possibility for the determination of the interaction radius from the emulsion experiment. Using the values of A, B and C given in Table 7 we calculate the interaction radii ( $R_p^*$ ) from the experimental IMFPs[18] and the results are given together with IMFPs in Table 8. While the ambiguity due to the experimental error is large, we obtain reasonable agreement between calculated $R_p$ and derived $R_p^*$.

VI. Discussion and summary

First of all, let us consider the effect of nuclear deformation in nucleus-nucleus scattering, especially for $^{11}Li$-$^{12}C$ scattering. We expect the following three possible deformation effects on the size of the $^{11}Li$ nucleus in a cylindrically symmetric deformed harmonic oscillator well with a positive quadratic deformation $\delta$. The harmonic oscillator constants are given by $\omega_x^2 = \omega_y^2 = \omega_o^2(1+\frac{2}{3}\delta)$, $\omega_z^2 = \omega_o^2(1-\frac{4}{3}\delta)$ while $\omega_{sph}/\omega_o = \left[1-\frac{4}{3}\delta^2-\frac{16}{27}\delta^3\right]^{1/6}$ from the requirement of volume conservation[20].

(a). The ratio of the effective area of the equi-potential surface of the deformed nucleus ( $S_{df}$ ) to that of the spherical nucleus ( $S_{sph}$ ) is given by

$$R_a = S_{df}/S_{sph} = \frac{1}{2}\left(\gamma^2+\frac{1}{\gamma}\right)\left[1+(\tfrac{1}{2})^2\kappa^2+(\tfrac{1}{2\cdot 4})^2\kappa^4+\ldots\right.$$

$$\left.+\left(\frac{(2r-3)!!}{(2r)!!}\right)^2\kappa^{2r}+\ldots\right], \quad (18)$$

where $\gamma = \left[(3-4\delta)/(3+2\delta)\right]^{1/6}$, and $\kappa = (1-\gamma^3)/(1+\gamma^3)$.

This expression is similar to eq.(3.3 ) of reference 21).

(b). If the ground state of $^{11}Li$ nucleus is given by the $(1s)^4(1p)^7$ configuration of deformed single particle wave-functions, the ratio of its mean square ( ms ) matter radius to the spherical one can be expressed by

$$R_b = \langle r^2\rangle_{dsm}/\langle r^2\rangle_{ssm} = \frac{2}{47}\left(15\gamma+\frac{17}{2}\frac{1}{\gamma^2}\right), \quad (19)$$

where the subscripts dsm and ssm stand for the deformed and spherical shell models respectively.

(c). The third possibility is that the ground state of $^{11}$Li may be expressed by the coexistence of the spherical shell model state ( $(1s)^4(1p)^7$ ) and deformed 3p-2h state ( $(1s)^4(1p)^5(2s1d)^2$ ), such that

$$|^{11}\mathrm{Li}\rangle = \sqrt{1-B^2}\,|(1s)^4(1p)^7:\mathrm{ssm}\rangle + B\,|3p\text{-}2h:\mathrm{dsm}\rangle , \qquad (20)$$

where B is the amplitude of the deformed 3p-2h state. Then, the ratio of the ms radii between the coexistence model ( cm ) and spherical shell model can be shown to be

$$R_c = \langle r^2\rangle_{cm}/\langle r^2\rangle_{ssm} = 1 + B^2\left(\frac{26}{47}\delta + \frac{251}{47}\delta^2 - 1\right). \qquad (21)$$

A similar expression has been employed in the study of the isotope dependence of the rms charge radii of Ca[22].

The dependence of the ratios of the effective areas R on the deformation parametr $\delta$ for the cases (a), (b) and (c) for mixing probabilities $B^2$ = 0.1, 0.2 and 0.3 are calculated and the results are shown in Fig. 3. For small values of $\delta$ the ratios for all the three cases appear to be approximately constant, very significant changes occur only for $\delta > 0.6$. Indeed, to account for the 17 % increment of the interaction cross section for $^{11}$Li-$^{12}$C scattering we find that $\delta$s' must be taken to be 0.74 for case (a) and 0.69 for case (b), while for case (c) $\delta$= 0.75, 0.74 and 0.72 for

mixing of $B^2$ =0.1, 0.2 and 0.3 respectively. On the other hand, if $^{12}C$ is assumed to have a same deformation parameter as that for $^{11}Li$, we need the $\delta$s to take values of 0.715, 0.615, 0.745, 0.705 and 0.655 for case (a), case (b) and the three different cases of (c) with $B^2$ = 0.1, 0.2 and 0.3 respectively. In all cases we need a large deformation parameter to explain the interaction cross section, and more information and study on the $^{11}Li$ nucleus are required in order to improve our understanding on the effects of deformation on the interaction cross section. Part of the underestimation in the interaction cross sections for S, Ta and U target nuclei as shown in Table 3 may be analogously explained by invoking the effects of nuclear deformation.

Next, we consider the mass number dependence of the interaction radii. Thus far the interaction cross section has been studied with the semiempirical formula[23]

$$\sigma_{int}(p,t) = \pi r_o^2 ( A_p^{1/3} + A_t^{1/3} - \Delta )^2, \qquad (22)$$

where $r_o$ = 1.29 fm and

$$\Delta = 1.0 - 0.028 A_{min} \text{ fm} \quad \text{with} \quad A_{min} = \text{Min}(A_p, A_t)$$
$$= 0 \text{ fm} \quad \text{for} \quad A_{min} > 30. \qquad (23)$$

Here, the "overlap parameter" $\Delta$ is meant to represent the diffuseness and partial transparency of the nuclear surfaces. Thus, comparing eqs.(13) and (22), we obtain the

semiempirical formula for the interaction radius

$$R_p = r_o A^{1/3} - \Delta/2. \qquad (24)$$

We plot the interaction radii ( from Table 6 ) as a function of $A^{1/3}$ in Fig. 3, and compare those with the semiempirical formula given by eq.(24). Reasonable agreement is obtained between and with a least square fitting program SALS[24] we obtain the expression

$$R_p = 1.355A^{1/3} - 0.365 \text{ fm}. \qquad (25)$$

Here, we wish stress the important implication of the interaction radius $R_p$ given by eqs.(24,25). While the semiempirical formula eq.(22) for the interaction cross section is known, the values of $r_o$ and $\Delta$ are not uniquely determined, because these parameters are coupled in eq.(22). On the other hand, the additivity relationship, eq.(13), indicates that the parameters $r_o$ and $\Delta$ should be defined for both the projectile nucleus $A_p$ and the target nucleus $A_t$. Therefore, the values of $r_o$ and $\Delta$, or equivalently $R_p$, should be considered as characteristic quantities of the nucleus. Furthermore, since the interaction cross sections of nuclei are essentially independent of energy from 0.1 to 30 GeV/N[23], the interaction radius $R_p$ can thus be considered as an energy independent characteristic nuclear radius in nucleus-nucleus scattering ( like the charge radius in

electron scattering ). Since we do not yet know at what (low) energy the idea of interaction radius breaks down, it would be quite interesting to study low energy nucleus-nucleus scattering in terms of the interaction radius, in particular the energy dependence of $r_o$ ( and $\Delta$ ) which changes from 1.355 fm in high energy scattering to 1.17 fm in the low energy optical potential[25].

In summary, we conclude that the experimental interaction cross sections and the IMFP of the projectile nucleus in the emulsion are generally well reproduced by the realistic Glauber model calculation using realistic nuclear wave functions. The nice agreement between experiment and theory can provide us with simple but quite powerful methods to determine the interaction radii of all nuclei. It may thus provide a means to investigate the consistency between nuclear physics for stable nuclei and that for nuclei far from stability. Furthermore, this kind of analysis may provide us a significant reference in the study of the anomously short IMFP phenomena[16,18].

The authors would like to thank Profs. K. Sugimoto and N. Takahashi, I. Tanihata and members of the INS-LBL Collaboration for their comments and discussions. They would like to thank Dr. C. Nagoshi for her comment and discussion on emulsion, and they also thank Prof. W. K. Koo for careful reading of the manuscript. One of the authors ( H.S. ) thanks Prof. M. Muraoka for his hospitality. The numerical calculation is performed with FACOM M380 at INS.

References


1). I. Tanihata et al., Phys. Lett. 160B (1985) 380.

2). I. Tanihata et al., Phys. Rev. Lett. 55 (1985) 2676.

3). H. Sato and Y. Okuhara, Phys. Lett. 162B (1985) 217.

4). K. Yazaki, Nucl. Phys. A277 (1977) 189.

5). M. Beiner, H. Flocard, N. Van Giai and P. Quentin, Nucl. Phys. A238 (1975) 29.

6). D. Vautherin and D. M. Brink, Phys. Rev. C5 (1972) 626.

7). J. W. Negele and D. Vautherin, Phys. Rev. C5 (1972) 1472.

8). J. W. Negele and D. Vautherin, unpublished.

9). R. J. Glauber, in Lectures in Theoretical Physics, edited by W. E. Brittin and L. G. Dunham (Wiley-Interscience, New York, 1959) Vol.1, p315.

10). V. Franco and G. K. Varma, Phys. Rev. C15 (1977) 1375.

11). V. Franco and G. K. Varma, Phys. Rev. C18 (1978) 349.

12). D. V. Bugg et al., Phys. Rev. 146 (1966) 980, and T. J. Devlin et al., Phys. Rev. D8 (1973) 136.

13). G. Igo et al., Nucl. Phys. B3 (1967) 181.

14). G. D. Westfall et al., Phys. Rev. C19 (1979) 1315.

15). C. F. Powell, P. H. Fowler and D. H. Perkins, The Study of the Elementary Particles by the Photographic Method (Pergamon Press, Oxford, 1959).

16). E. M. Friedländer et al., Phys. Rev. Lett. 45 (1980) 1084.

17). W. H. Barkas, Nuclear Research Emulsions (Academic Press, New York, 1973) and C. Nagoshi, private communication.

18). R. Bhanja et al., Phys. Rev. Lett. 54 (1985) 771.

19). H. Sato and Y. Okuhara, Phy. Lett. B (1986)

20). B. E. Chi, Nucl. Phys. 83 (1966) 97.

21). Y. Yamaguchi, Prog. Theor. Phys. 67 (1982) 1810.

22). H. Sato, Nucl. Phys. A304 (1978) 477.

23). A. S. Goldhaber and H. H. Heckman, Annu. Rev. Nucl. Part. Sci. 28 (1979) 161.

24). T. Nakagawa and Y. Oyanagi, "Program System SALS for Nonlinear Least-Squares Fitting in Experimental Science" in Recent Developments in Statistical Inference and Data Analysis, ed. K.Matsushita (North Holland Publishing Company, 1980), p.221.

25). F. D. Becchetti and G. W. Greenlees, Phys. Rev. 182 (1969) 1190.

Figure Captions.

Fig.1. The interaction cross sections for the nucleus ($A_p$) - $^{12}C$ scatterings at 0.79 GeV/N calculated with the SKIII and SKV interactions and the experimental values by INS-LBL Collaboration[1,2]. The solid line with open circles is for the experimental values, the dotted line with solid squares is for the SKIII interaction, and the dash-dotted with solid circles is for the SKV interaction.

Fig.2. The IMFPs in Ilford G5 at 1.8 GeV/N calculated with the SKV interaction (solid circle) and the experimental IMFPs obtained with $^{40}Ar$ beam[18] (cross).

Fig.3. The deformation parameter dependence of the ratio of the effective areas between deformed nucleus and spherical nucleus calculated with eqs.(18), (19) and (21).

Fig.4. The mass number dependence of the interaction radii calculated at 1.8 GeV/N with the SKV interaction. The solid line shows the least square fitting (25) and dashed line corresponds to the semiempirical formula (24).

Table 1. The total and interaction cross sections (in mb) for nucleus-nucleus scattering at 0.79 GeV/N calculated with the SKV interaction.

| Nuclei | $\sigma_{tot}$ $\bar{\chi}_1$ | upto $\bar{\chi}_2$ | $\sigma_{int}$ $\bar{\chi}_1$ | upto $\bar{\chi}_2$ |
|---|---|---|---|---|
| p-$^{4}$He | 132 | 136 | 107 | 109 |
| $^{4}$He-$^{4}$He | 418 | 377 | 302 | 280 |
| p-$^{12}$C | 343 | 353 | 256 | 260 |
| $^{4}$He-$^{12}$C | 876 | 785 | 571 | 529 |
| $^{12}$C-$^{12}$C | 1545 | 1394 | 940 | 875 |
| p-$^{56}$Fe | 1162 | 1185 | 751 | 757 |
| $^{4}$He-$^{56}$Fe | 2180 | 1959 | 1289 | 1199 |
| $^{12}$C-$^{56}$Fe | 3211 | 2914 | 1835 | 1717 |
| $^{56}$Fe-$^{56}$Fe | 5524 | 5027 | 3054 | 2859 |
| p-$^{208}$Pb | 3094 | 3136 | 1819 | 1828 |
| $^{4}$He-$^{208}$Pb | 4738 | 4356 | 2655 | 2509 |
| $^{12}$C-$^{208}$Pb | 6235 | 5777 | 3432 | 3254 |
| $^{56}$Fe-$^{208}$Pb | 9377 | 8688 | 5063 | 4795 |
| $^{208}$Pb-$^{208}$Pb | 14288 | 13429 | 7601 | 7262 |

Table 2. The total and interaction cross sections (in mb) for proton-nucleus scattering at 1.00 GeV calculated with the SKIII and SKV interactions in comparison with experimental data.

| Target | $\sigma_{tot}$ | | | $\sigma_{int}$ | | |
|---|---|---|---|---|---|---|
| | $\sigma_{exp}$ [a] | $\sigma_{cal}$ [b] | $\sigma_{cal}$ [c] | $\sigma_{exp}$ [a] | $\sigma_{cal}$ [b] | $\sigma_{cal}$ [c] |
| $^{4}$He | 152± 8 | 139 | 139 | 111±10 | 111 | 111 |
| $^{6}$Li | 199± 11 | 200 | 203 | | 157 | 169 |
| C | 370± 9 | 356 | 361 | 258±17 | 257 | 263 |
| O | 475± 44 | 457 | 454 | 296±50 | 322 | 319 |
| $^{208}$Pb | 3155±450 | 3199 | 3184 | | 1838 | 1836 |

a). Ref. 13).

b). With the SKIII interaction.

c). With the SKV interaction.

Table 3. The interaction cross sections (in b) for $^{56}$Fe-nucleus scattering at 1.88 GeV/N calculated with the SKIII and SKV interactions in comparison with experimental data.

| Target | $\sigma_{int}$ | | |
|---|---|---|---|
| | $\sigma_{exp}$ a) | $\sigma_{cal}$ b) | $\sigma_{cal}$ c) |
| H | 0.75±0.05 | 0.765 | 0.768 |
| Li | 1.43±0.04 | 1.483 | 1.544 |
| Be | 1.67±0.05 | 1.592 | 1.651 |
| C | 1.66±0.06 | 1.725 | 1.758 |
| S | 2.22±0.09 | 2.437 | 2.448 |
| Cu | 2.94±0.10 | 3.055 | 3.087 |
| Ag | 3.71±0.14 | 3.704 | 3.723 |
| Ta | 4.97±0.20 | 4.544 | 4.587 |
| Pb | 5.10±0.27 | 4.857 | 4.884 |
| U | 5.92±0.29 | 5.119 | 5.179 |

a). Ref. 14).

b). With the SKIII interaction.

c). With the SKV interaction.

Table 4. The interaction cross sections (in mb) for nucleus-nucleus scattering at 0.79 GeV/N calculated with the SKIII and SKV interactions in comparison with experimental data.

| Target / Beam | $^{4}$He | | $^{9}$Be | | $^{12}$C | | $^{27}$Al | |
|---|---|---|---|---|---|---|---|---|
| | Theor. | Exp.[a] | Theor. | Exp.[a] | Theor. | Exp.[a] | Theor. | Exp.[a] |
| $^{4}$He (SKIII) | 282 | | 453 | | 521 | | 801 | |
| ( SKV ) | 280 | 262±19 | 473 | 485± 4 | 529 | 503± 5 | 809 | 780±13 |
| $^{6}$He (SKIII) | | | 592 | | 672 | | 984 | |
| ( SKV ) | | | 624 | 672± 7 | 689 | 722± 6 | 1004 | 1063± 8 |
| $^{8}$He (SKIII) | | | 704 | | 790 | | 1136 | |
| ( SKV ) | | | 713 | 757± 4 | 781 | 817± 6 | 1123 | 1197± 9 |
| $^{10}$He (SKIII) | | | | | | | | |
| ( SKV ) | | | 825 | | 899 | | 1266 | |
| $^{6}$Li (SKIII) | | | 567 | | 645 | | 952 | |
| ( SKV ) | | | 622 | 651± 8 | 688 | 688±12 | 1001 | 1010±11 |
| $^{7}$Li (SKIII) | | | 609 | | 690 | | 1008 | |
| ( SKV ) | | | 666 | 686± 4 | 735 | 736± 6 | 1059 | 1071± 7 |
| $^{8}$Li (SKIII) | | | 652 | | 735 | | 1065 | |
| ( SKV ) | | | 703 | 727± 6 | 773 | 768± 9 | 1108 | 1144± 8 |
| $^{9}$Li (SKIII) | | | 695 | | 780 | | 1123 | |
| ( SKV ) | | | 737 | 739± 5 | 807 | 796± 6 | 1153 | 1135± 8 |
| $^{11}$Li (SKIII) | | | 823 | | 918 | | 1289 | |
| ( SKV ) | | | 829 | | 902 | 1056±30 | 1269 | |
| $^{9}$Be (SKIII) | | | 673 | | 758 | | 1093 | |
| ( SKV ) | | | 731 | 756± 6 | 802 | 807± 9 | 1144 | 1176±11 |
| $^{10}$Be (SKIII) | | | 709 | | 796 | | 1141 | |
| ( SKV ) | | | 760 | 766± 8 | 831 | 825±10 | 1181 | 1180±16 |

a). Ref. 1) and Ref. 2).

Table 5. The additivity relationship for $^{56}$Fe-nucleus and $^{4}$He-nucleus interaction cross sections (in b) at 1.88 GeV/N calculated by RHS and LHS of eq.(13) with the SKV interaction.

| Target | $^{56}$Fe-A | | $^{4}$He-A | |
|---|---|---|---|---|
| | $\sigma_{int}$ | $\pi(R_p+R_t)^2$ | $\sigma_{int}$ | $\pi(R_p+R_t)^2$ |
| $^{7}$Li | 1.548 | 1.562 | 0.435 | 0.440 |
| $^{9}$Be | 1.651 | 1.662 | 0.488 | 0.494 |
| $^{12}$C | 1.758 | 1.766 | 0.545 | 0.552 |
| $^{32}$S | 2.448 | 2.448 | 0.933 | 0.957 |
| $^{65}$Cu | 3.094 | 3.107 | 1.337 | 1.384 |
| $^{109}$Ag | 3.744 | 3.747 | 1.770 | 1.821 |
| $^{184}$W | 4.610 | 4.619 | 2.371 | 2.443 |
| $^{208}$Pb | 4.884 | 4.894 | 2.560 | 2.644 |
| $^{238}$U | 5.179 | 5.191 | 2.777 | 2.863 |

Table 6. The rms matter ($r_{rms}$) and interaction ($R_p$) radii and IMFPs ($\lambda_p$) of projectile nuclei in the emulsion at 1.88 GeV/N calculated with SKV interaction.

| Proj. | $r_{rms}$ | $R_p$ | $\lambda_p^{a)}$ | $\lambda_p^{b)}$ | Proj. | $r_{rms}$ | $R_p$ | $\lambda_p^{a)}$ | $\lambda_p^{b)}$ |
|---|---|---|---|---|---|---|---|---|---|
| $^{4}He$ | 1.76 | 1.52 | 18.8 | 18.4 | $^{31}P$ | 3.14 | 3.93 | 8.7 | 8.4 |
| $^{6}He$ | 2.47 | 2.07 | 15.5 | 15.2 | $^{32}S$ | 3.18 | 4.00 | 8.6 | 8.2 |
| $^{8}He$ | 2.43 | 2.38 | 14.0 | 13.6 | $^{34}S$ | 3.23 | 4.08 | 8.4 | 8.0 |
| $^{6}Li$ | 2.48 | 2.07 | 15.6 | 15.2 | $^{35}Cl$ | 3.26 | 4.12 | 8.3 | 8.0 |
| $^{7}Li$ | 2.45 | 2.23 | 14.7 | 14.3 | $^{37}Cl$ | 3.29 | 4.18 | 8.2 | 7.8 |
| $^{8}Li$ | 2.44 | 2.35 | 14.1 | 13.7 | $^{36}Ar$ | 3.28 | 4.16 | 8.2 | 7.9 |
| $^{9}Be$ | 2.44 | 2.45 | 13.6 | 13.3 | $^{38}Ar$ | 3.31 | 4.21 | 8.1 | 7.8 |
| $^{10}Be$ | 2.43 | 2.54 | 13.2 | 12.9 | $^{40}Ar$ | 3.37 | 4.30 | 7.9 | 7.6 |
| $^{10}B$ | 2.44 | 2.54 | 13.3 | 12.9 | $^{39}K$ | 3.33 | 4.24 | 8.0 | 7.7 |
| $^{11}B$ | 2.44 | 2.61 | 13.0 | 12.6 | $^{41}K$ | 3.38 | 4.32 | 7.9 | 7.5 |
| $^{12}C$ | 2.44 | 2.67 | 12.7 | 12.3 | $^{40}Ca$ | 3.34 | 4.26 | 8.0 | 7.7 |
| $^{13}C$ | 2.49 | 2.77 | 12.3 | 11.9 | $^{44}Ca$ | 3.44 | 4.41 | 7.7 | 7.4 |
| $^{14}N$ | 2.54 | 2.85 | 12.0 | 11.6 | $^{48}Ca$ | 3.51 | 4.53 | 7.5 | 7.1 |
| $^{15}N$ | 2.56 | 2.92 | 11.7 | 11.4 | $^{56}Fe$ | 3.69 | 4.82 | 6.9 | 6.6 |
| $^{16}O$ | 2.58 | 2.98 | 11.5 | 11.1 | $^{58}Ni$ | 3.72 | 4.86 | 6.9 | 6.6 |
| $^{18}O$ | 2.72 | 3.17 | 10.9 | 10.5 | $^{63}Cu$ | 3.84 | 5.08 | 6.5 | 6.2 |
| $^{19}F$ | 2.78 | 3.25 | 10.6 | 10.2 | $^{65}Cu$ | 3.88 | 5.12 | 6.4 | 6.2 |
| $^{20}Ne$ | 2.83 | 3.33 | 10.4 | 10.0 | $^{79}Br$ | 4.11 | 5.48 | 5.9 | 5.6 |
| $^{22}Ne$ | 2.89 | 3.44 | 10.0 | 9.7 | $^{81}Br$ | 4.14 | 5.52 | 5.9 | 5.6 |
| $^{23}Na$ | 2.92 | 3.50 | 9.9 | 9.5 | $^{107}Ag$ | 4.51 | 6.04 | 5.2 | 5.0 |
| $^{24}Mg$ | 2.94 | 3.55 | 9.7 | 9.4 | $^{109}Ag$ | 4.54 | 6.10 | 5.1 | 4.9 |
| $^{25}Mg$ | 2.96 | 3.60 | 9.6 | 9.2 | $^{120}Sn$ | 4.67 | 6.29 | 4.9 | 4.7 |
| $^{26}Mg$ | 2.98 | 3.64 | 9.5 | 9.1 | $^{127}I$ | 4.77 | 6.40 | 4.8 | 4.6 |
| $^{27}Al$ | 3.00 | 3.68 | 9.4 | 9.0 | $^{181}Ta$ | 5.36 | 7.27 | 4.1 | 3.9 |
| $^{28}Si$ | 3.02 | 3.72 | 9.3 | 8.9 | $^{184}W$ | 5.39 | 7.30 | 4.0 | 3.8 |
| $^{29}Si$ | 3.06 | 3.79 | 9.1 | 8.7 | $^{208}Pb$ | 5.56 | 7.66 | 3.8 | 3.6 |
| $^{30}Si$ | 3.09 | 3.86 | 8.9 | 8.6 | $^{238}U$ | 5.87 | 8.03 | 3.5 | 3.3 |

Units: $r_{rms}$ in fm, $R_p$ in fm and $\lambda_p$ in cm.
Emulsions: a) Ilford G5 and b) Fuji ET7B.

Table 7. The coefficients A, B and C of eq.(16) for the IMFP in the emulsions at 1.88 GeV/N calculated with the SKV interaction.

| Emulsion | A | B | | | | | C | | |
|---|---|---|---|---|---|---|---|---|---|
| | | (a) | (b) | (c) | (d) | (e) | (a) | (b,c,d,e) | |
| Ilford G5 | 2.47 | 1.28 | 1.24 | 1.23 | 1.22 | 1.21 | 2.81 | 2.80 | |
| | | (a) | (b) | (c) | (d) | (e) | (a) | (b,c) | (d,e) |
| Fuji ET7B | 2.65 | 1.33 | 1.29 | 1.28 | 1.27 | 1.26 | 2.80 | 2.79 | 2.78 |

*Units:* A in $10^{-3}$/cmfm$^2$, B in $10^{-2}$/cmfm and C in $10^{-2}$/cm for the IMFP in cm and the $R_p$ in fm.

Projectiles: (a) $^4$He, (b) 1p shell nucleus, (c) 2s1d shell nucleus, (d) A = 50∼150 nucleus and (e) heavier nucleus.

Table 8. The experimental IMFPs in Ilford G5 with 1.8 GeV/N $^{40}Ar$ beam[18] and the derived interaction radii.

| Projectile. | $\lambda_p$ | $R_p^*$ |
|---|---|---|
| He | 19.52 ± 0.65 | 1.42 ± 0.09 |
| Li | 14.67 ± 1.39 | 2.24 ± 0.28 |
| Be | 13.15 ± 1.46 | 2.56 ± 0.34 |
| B | 14.79 ± 1.71 | 2.21 ± 0.34 |
| C | 11.73 ± 1.20 | 2.92 ± 0.33 |
| N | 10.29 ± 1.21 | 3.34 ± 0.40 |
| O | 13.43 ± 1.65 | 2.50 ± 0.37 |
| F | 11.31 ± 1.33 | 3.04 ± 0.38 |
| Ne | 13.06 ± 1.71 | 2.59 ± 0.40 |
| Na | 11.68 ± 1.44 | 2.94 ± 0.40 |
| Mg | 11.19 ± 1.46 | 3.08 ± 0.43 |
| Al | 8.36 ± 1.04 | 4.09 ± 0.46 |
| Si | 8.93 ± 1.12 | 3.85 ± 0.45 |
| P | 8.99 ± 1.02 | 3.82 ± 0.41 |
| S | 9.72 ± 1.07 | 3.55 ± 0.38 |
| Cl | 8.07 ± 0.99 | 4.22 ± 0.46 |
| Ar | 10.50 ± 0.87 | 3.29 ± 0.28 |
| $^{40}Ar$[a)] | 8.97 ± 0.16 | 3.83 ± 0.06 |

Units: the IMFP $\lambda_p$ in cm and the $R_p^*$ in fm.

a). The primary beam.

Fig. 1

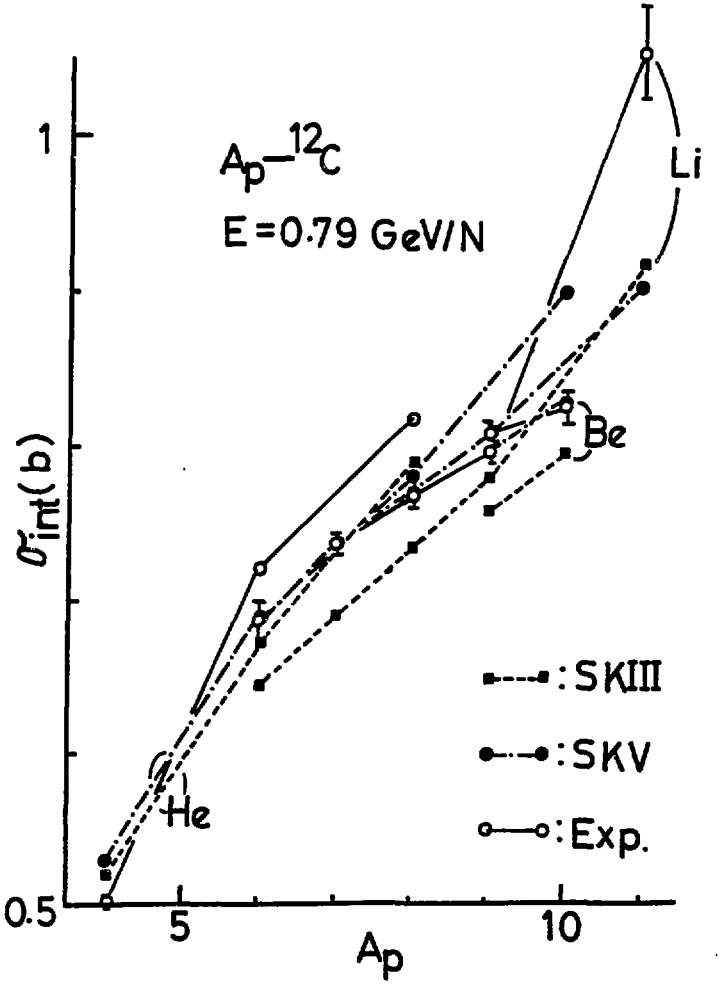

Fig. 2

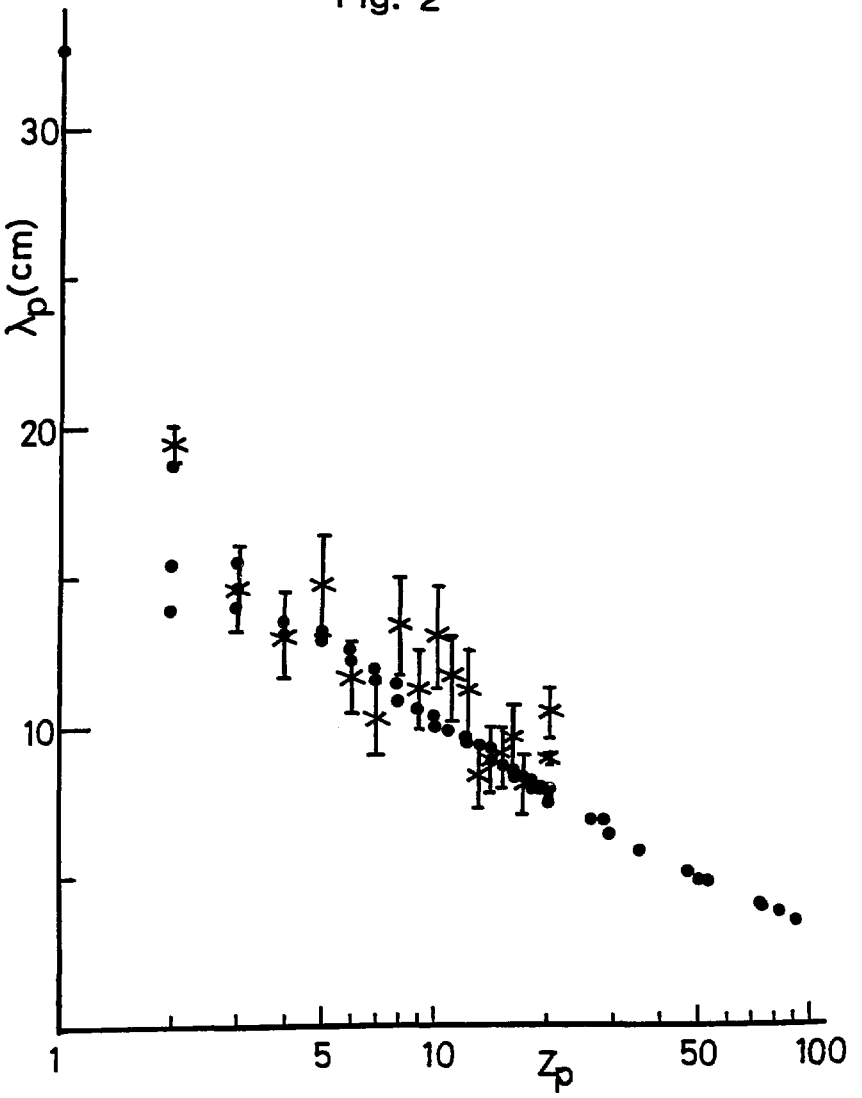

Fig. 3

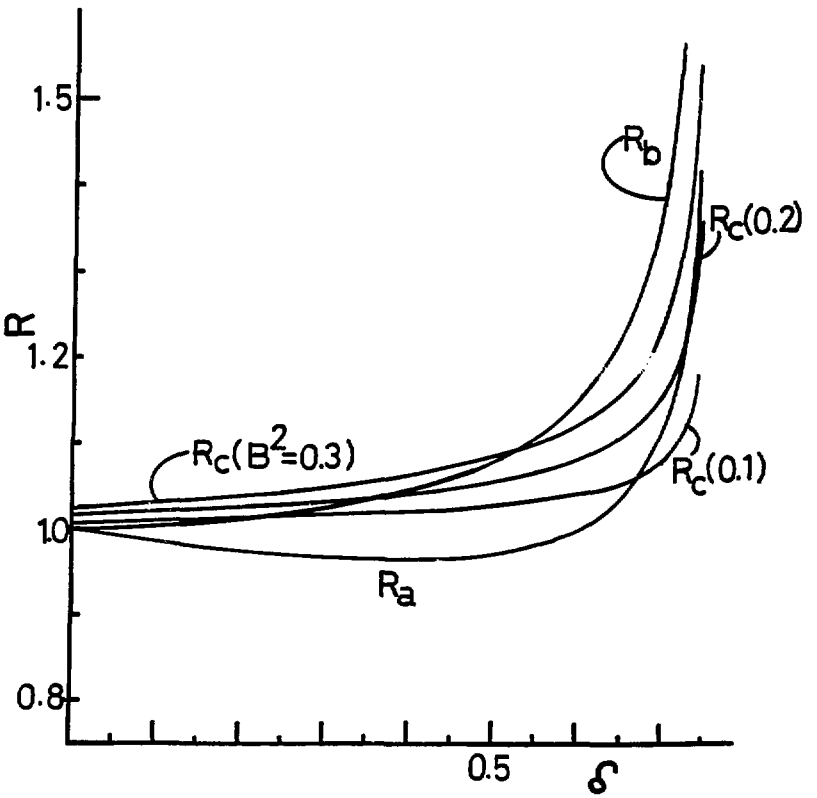

Fig. 4